Inorganic Chemistry

pubs.acs.org/IC

Article

Luminescence and Scintillation of $[Nb_2O_2F_9]^{3-}$-Dimer-Containing Oxide–Fluorides: $Cs_{10}(Nb_2O_2F_9)_3F$, $Cs_{9.4}K_{0.6}(Nb_2O_2F_9)_3F$, and $Cs_{10}(Nb_2O_2F_9)_3Cl$

Gyanendra B. Ayer, Gregory Morrison, Mark D. Smith, Luiz G. Jacobsohn, and Hans-Conrad zur Loye*

Cite This: *Inorg. Chem.* 2022, 61, 3256–3262

Read Online

ACCESS | Metrics & More | Article Recommendations | Supporting Information

ABSTRACT: We report three novel Nb-containing oxide–fluorides, $Cs_{10}(Nb_2O_2F_9)_3F$, $Cs_{9.4}K_{0.6}(Nb_2O_2F_9)_3F$, and $Cs_{10}(Nb_2O_2F_9)_3Cl$, which were prepared as high-quality single crystals via a HF-based mild hydrothermal route. The compounds all crystallize in the trigonal crystal system with space group $P\bar{3}m1$. All three compositions form the same framework structure consisting of isolated $[Nb_2O_2F_9]^{3-}$ dimers that create hexagonal channels that are occupied by disordered halide species. Upon excitation by UV light at room temperature, these compounds display broad band emission with a maximum at 440 nm for $Cs_{10}(Nb_2O_2F_9)_3F$. The broad band emission of these compounds is attributed to the charge-transfer transitions of Nb–O bonds within the $[Nb_2O_2F_9]^{3-}$ dimers. All three compounds scintillate blue under X-ray irradiation. Radioluminescence (RL) measurements performed on $Cs_{10}(Nb_2O_2F_9)_3F$ demonstrate that the RL emission intensity decreases with increasing temperature and that the integrated RL emission (300–750 nm) is 4% of $Bi_4Ge_3O_{12}$ (BGO) powder. Thermogravimetric analysis confirms that $Cs_{10}(Nb_2O_2F_9)_3F$ has excellent thermal stability up to 600 °C and no structural phase transition is observed prior to sample decomposition.

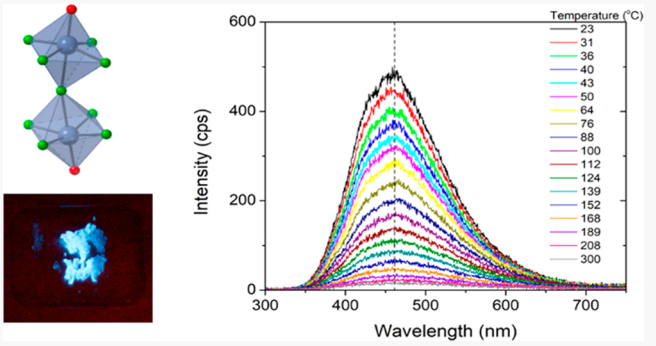

INTRODUCTION

Scintillators capable of converting high-energy ionizing radiation into low-energy visible photons continue to generate great interest because they are widely used in radiation detection and X-ray radiography,[1] medical imaging,[2] including positron emission tomography[3] and computer tomography scanners,[4] and geophysical exploration.[5] Different scintillating materials are reported for various applications, such as NaI:Tl, CsI:Tl, $Lu_2SiO_5:Ce^{3+}$, $Cs_4SrI_6:Eu^{2+}$, $CdWO_4$, and $Bi_4Ge_3O_{12}$ (BGO).[6−11] However, there are still limitations on more widespread use, such as the high cost, hygroscopicity, and stability issues of existing materials. Recently, several compounds containing mixed-anion oxide–halides have been reported as efficient X-ray scintillators with high quantum yield. The low cost along with high stability of these materials makes them of interest for investigation as new radiation detection and scintillation materials.[12−15]

Compounds containing metals with a d^0 electron configuration, such as Nb^{5+}, can exhibit intense luminescence and scintillation. Bulk niobates with the composition $LnMO_4$ (Ln = lanthanide element; M = V, Nb, Ta) are dense materials with potential for the detection of X-rays.[16] Moreover, gadolinium tantaloniobate, $GdNb_{0.2}Ta_{0.8}O_4$, crystallizing in the fergusonite structure, is a promising material because of its high radiation stopping power.[17] β-$BiNbO_4$, synthesized by a solid-state route, has been investigated as an efficient luminescent material that emits intense blue light at 435 nm under UV light and X-ray excitation.[18] Also, single crystals of the complex niobates Sr_3NaNbO_6 and $GdKNaNbO_5$ exhibit violet emission at room temperature when excited by UV light at 250 nm.[19,20] An extension to these materials, representing a potential novel class of luminescing materials, is mixed-anion oxide–fluorides, in which Nb acts as the intrinsic luminescence center. Quaternary Nb-based oxide–fluorides, such as $BaNbOF_5$ and Cs_2NbOF_5, which possess isolated $NbOF_5$ octahedra, are reported to be excellent blue emitters, ascribed to the charge-transfer transitions of Nb–O bonds in the $[NbOF_5]^{2-}$ units.[21,22] While the luminescence properties of Nb-based compounds containing isolated octahedra $[NbO_6/NbOF_5]$ have been studied, to the best of our knowledge, there have been no reports on compounds containing $[Nb_2O_2F_9]^{3-}$ dimers that exhibit optical emission. This motivated us to

Received: December 6, 2021
Published: February 9, 2022

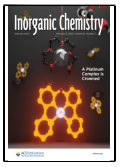

https://doi.org/10.1021/acs.inorgchem.1c03787
Inorg. Chem. 2022, 61, 3256–3262

Table 1. Crystallographic Data for $Cs_{10}(Nb_2O_2F_9)_3F$, $Cs_{9.4}K_{0.6}(Nb_2O_2F_9)_3F$, and $Cs_{10}(Nb_2O_2F_9)_3Cl$

	$Cs_{10}(Nb_2O_2F_9)_3F$	$Cs_{9.4}K_{0.6}(Nb_2O_2F_9)_3F$	$Cs_{10}(Nb_2O_2F_9)_3Cl$
fw (g mol^{-1})	2514.56	2457.34	2531.01
cryst syst	trigonal	trigonal	trigonal
space group	$P\bar{3}m1$	$P\bar{3}m1$	$P\bar{3}m1$
a, Å	21.3033(4)	21.1100(5)	21.3283(6)
b, Å	21.3033(4)	21.1100(5)	21.3283(6)
c, Å	8.4899(2)	8.4310(3)	8.4974(3)
γ, deg	120	120	120
V, Å^3	3336.77(15)	3253.76(19)	3347.6(2)
ρ_{calcd}, g cm^{-3}	3.754	3.762	3.766
radiation (λ, Å)		Mo Kα (0.71073)	
μ, mm^{-1}	9.694	9.495	9.718
T, K		300(2)	
cryst dimens, mm^3	0.12 × 0.07 × 0.07	0.10 × 0.08 × 0.08	0.14 × 0.05 × 0.04
2θ range, deg	2.6409−34.5983	2.228−36.422	2.638−32.276
reflns collected	307773	178256	130488
data/restraints/param	5762/2/148	5603/2/179	4366/1/151
$\Delta\rho_{max}$ (e Å^{-3})	2.634	2.322	1.568
$\Delta\rho_{min}$ (e Å^{-3})	−2.202	−0.990	−1.614
R_{int}	0.0453	0.0432	0.0462
GOF	1.055	1.144	1.068
R_1 [$I > 2\sigma(I)$]	0.0314	0.0343	0.0256
wR_2 (all data)	0.0889	0.0882	0.0669

explore novel Nb-based oxide−fluoride host matrixes toward the development of new luminescent materials.

Herein, we report three new Nb-based mixed-anion oxide−fluoride compounds, $Cs_{10}(Nb_2O_2F_9)_3F$, $Cs_{9.4}K_{0.6}(Nb_2O_2F_9)_3F$, and $Cs_{10}(Nb_2O_2F_9)_3Cl$, which can easily be prepared via a hydrofluoric acid (HF)-based mild hydrothermal route at 160 °C. All three compounds crystallize in the trigonal space group $P\bar{3}m1$ and consist of isolated $[Nb_2O_2F_9]^{3-}$ dimers that are linked together through Cs ions to form a complex 3D framework structure. These compounds exhibit broad blue emission under UV-light excitation with a maximum at 440 nm for $Cs_{10}(Nb_2O_2F_9)_3F$. Furthermore, single crystals of all three phases scintillate and emit intense blue light upon exposure to laboratory X-rays. The scintillation behavior of $Cs_{10}(Nb_2O_2F_9)_3F$ was characterized by radioluminescence (RL) measurements, which determined that the integral RL emission was about 4% of BGO powder.

EXPERIMENTAL SECTION

Reagents. CsF (Alfa Aesar, 99.9%), CsCl (Alfa Aesar, 99%), Nb_2O_5 (Alfa Aesar, 99.5%), $KNbO_3$ (Johnson Matthey Inc., 99.9%), and HF (EMD, 49%) were used as received.

Warning! *HF should only be handled in a well ventilated space, and proper safety precautions must be used. If contact with the liquid or vapor occurs, proper treatment procedures should immediately be followed.*

Synthesis. Single crystals of the title compounds were grown using a mild hydrothermal route. For the preparation of $Cs_{10}(Nb_2O_2F_9)_3F$ and $Cs_{10}(Nb_2O_2F_9)_3Cl$, 0.5 mmol of Nb_2O_5, 0.5 mL of 49% HF, and 1.5 mL of H_2O were combined with 4 mmol of CsF and CsCl, respectively. For the synthesis of $Cs_{9.4}K_{0.6}(Nb_2O_2F_9)_3F$, 4 mmol of CsF and 1 mmol of $KNbO_3$ were combined with 1.5 mL of H_2O and 0.5 mL of 49% HF. The respective solutions were placed in 23 mL polytetrafluoroethylene (PTFE) liners, which were then sealed into stainless steel autoclaves, heated to 160 °C at a rate of 5 °C min^{-1}, held at this temperature for 24 h, and cooled to room temperature at a rate of 6 °C h^{-1}. The mother liquor was decanted from the single-crystal products, which were further isolated by filtration and washed with water and acetone. In all cases, the reaction yielded a single-phase product consisting of colorless rod crystals with 100% yield based on the Nb precursors.

Powder X-ray Diffraction (PXRD). PXRD data for phase purity confirmation were collected on polycrystalline powders prepared by grinding product single crystals into a fine powder. X-ray diffraction (XRD) patterns were collected on a Bruker D2 PHASER diffractometer utilizing Cu Kα radiation. The data were collected over the range from 5 to 65° in 2θ with a step size of 0.02°. While the PXRD patterns of the products indicated no secondary phases, they, however, exhibited a preferred orientation due to the rod shape of the crystals, which persisted even after grinding (Figures S1−S3).

Single-Crystal XRD. Single-crystal XRD data from colorless rod crystals were collected at 301(2) K using a Bruker D8 QUEST diffractometer equipped with a PHOTON-II area detector and an Incoatec microfocus source (Mo Kα radiation; λ = 0.71073 Å).[21] The data collection for $Cs_{10}(Nb_2O_2F_9)_3F$, $Cs_{9.4}K_{0.6}(Nb_2O_2F_9)_3F$, and $Cs_{10}(Nb_2O_2F_9)_3Cl$ covered 99.9%, 99.4%, and 99.9% of the reciprocal space to $2\theta_{max}$ = 72.7°, 72.8°, and 65.2°, with average reflection redundancies of 53.4, 31.8, and 16.0, respectively, after absorption correction. The raw area detector dataframes were reduced and corrected for absorption effects using the *SAINT+* and *SADABS* programs.[23,24] The final unit cell parameters were determined by least-squares refinement of 9294, 9745, and 9000 reflections for $Cs_{10}(Nb_2O_2F_9)_3F$, $Cs_{9.4}K_{0.6}(Nb_2O_2F_9)_3F$, and $Cs_{10}(Nb_2O_2F_9)_3Cl$, respectively. An initial structural model was obtained with *SHELXT*.[25] Subsequent difference Fourier calculations and full-matrix least-squares refinement against F^2 were performed with *SHELXL-2018*[26] using *OLEX2*.[27] The single-crystal XRD data and results of the diffraction experiments are summarized in Table 1.

Luminescence Properties. Photoluminescence (PL) spectra were collected on a powdered sample of $Cs_{10}(Nb_2O_2F_9)_3F$ using a PerkinElmer LS55 luminescence spectrometer. Excitation spectra were collected at an emission wavelength of 440 nm, and the emission scan was collected at an excitation wavelength of 248 nm. A photograph showing the scintillation of $Cs_{10}(Nb_2O_2F_9)_3F$ was obtained using a Rigaku Ultima IV diffractometer equipped with Cu Kα (λ = 1.54018 Å) as the excitation source. RL measurements were executed using a customer-designed configuration of the Freiberg Instruments Lexsyg Research spectrofluorometer equipped with a Varian Medical Systems VF-50J X-ray tube with a W target. The X-ray source was coupled with an ionization chamber for

https://doi.org/10.1021/acs.inorgchem.1c03787
Inorg. Chem. 2022, 61, 3256−3262

continuous radiation intensity monitoring. The light emitted by the sample was collected by an Andor Technology SR-OPT-8024 optical fiber connected to an Andor Technology Shamrock 163 spectrograph coupled to a cooled (−80 °C) Andor Technology DU920P-BU Newton CCD camera (spectral resolution = ∼0.5 nm pixel^{-1}). Powders filled ca. 8-mm-diameter 0.5-mm-deep cups, thus allowing for a relative RL intensity comparison between different samples. BGO powder [Alfa Aesar Puratronic, 99.9995% (metals basis)] was used as the reference. RL was measured under continuous X-ray irradiation (40 kV, 1 mA) by a broad range of X-rays including both W lines and bremsstrahlung radiation with integration times of 1, 5, or 10 s. RL measurements as a function of the temperature were executed under a continuous 0.5 °C s^{-1} heating rate up to 500 °C and 4 s of integration time. Thus, the temperature increased by 2 °C during the acquisition of each spectrum. Spectra were labeled by the starting acquisition temperature. All spectra were automatically corrected by the spectral response of the system determined by the manufacturer.

Crystal Growth. Single crystals of the title compounds $Cs_{10}(Nb_2O_2F_9)_3F$, $Cs_{9.4}K_{0.6}(Nb_2O_2F_9)_3F$, and $Cs_{10}(Nb_2O_2F_9)_3Cl$ were grown via a HF-based mild hydrothermal route. This technique has been found to be effective in synthesizing a large number of complex fluorides and oxide−fluorides, with novel structural motifs.[15,28−33] The single-phase products for all compounds were obtained by using similar reaction conditions but different Cs and Nb precursors. It is well-known that the specific precursor in mild hydrothermal routes can drastically affect the reaction outcome. Attempts to obtain the Ta analogues using similar reaction conditions and exploring different precursors were unsuccessful and only resulted in the formation of the reported ternary $CsTaF_6$ compound.[34]

The simple HF(aq)-based synthetic route that results in the title compounds avoids the use of F_2 or HF gas as a fluorinating reagent. In the crystal growth reactions, HF acts as both the F source and a mineralizer, which digests the starting reagents and favors the formation of a stable oxide−fluoride structure. Previous studies have shown that niobium oxides are highly soluble in HF and do not form polymeric species in a fluoride solution.[35] However, quaternary or higher extended compounds can be synthesized from such HF solutions by mixing soluble precursors into the Nb solution, where the composition and structure of the product formed depends on the precursor materials added. The concentration of HF also plays a significant role in determining the composition of the product formed. We observed that the reaction outcome can be shifted toward the target phase by utilizing a low HF concentration (∼ 40%), while at a high HF concentration (∼49%), the reaction significantly favors the formation of the ternary $CsNbF_6$ compound.[34] By comparison, Tananaev and Savchenko, who investigated the synthesis of K_2NbF_7 in a HF solution with a concentration of about 42%, found that high HF concentrations result in the precipitation of $KNbF_6$.[35]

F^- and O^{2-} ions are aliovalent and can both fit into the same crystallographic environments because of their almost identical ionic radii. The incorporation of F for O ions impacts the electronic structure of the materials and leads to different properties. The pronounced effect of F incorporation is exemplified by $BaWO_4$, which exhibits enhanced scintillation behavior once fluorinated to a composition of $BaWO_2F_4$.[15] These observations demonstrate that the HF-based mild hydrothermal method is effective for the synthesis of various oxide−fluorides and also that the actual reaction chemistry is complex, and the associated mechanism has rarely been studied to date.

Crystal Structure. The title compounds $Cs_{10}(Nb_2O_2F_9)_3F$, $Cs_{9.4}K_{0.6}(Nb_2O_2F_9)_3F$, and $Cs_{10}(Nb_2O_2F_9)_3Cl$ crystallize in the trigonal space group $P\bar{3}m1$ and represent a new series of mixed-anion oxide−fluoride compounds. These compounds are new members of the $A_{10}(Nb_2O_2F_9)_3X$ (A = K, Rb, Cs, NH_4; X = F, Cl) family.[36] The three reported compounds all crystallize in the same structure type as the previously reported Rb and NH_4 compounds, whereas the previously reported K compound forms in an orthorhombic distortion of the same structure type. Although the three reported compounds possess three different compositions, they are structurally quite similar and exhibit only minor differences in the site occupants of a single column within a channel by unique halide ions. Each Nb site forms a $NbOF_5$ coordination polyhedron in the shape of an octahedron, with Nb−O distances ranging from 1.689(9) to 1.719(6) Å and Nb−F distances of 1.741(19)−2.199(4) Å. In all three cases, two $NbOF_5$ polyhedra vertex-share F atoms to form $[Nb_2O_2F_9]^{3-}$ dimeric units (Figure 1a), which are isolated from one another but linked together by Cs ions to form a 3D framework structure (Figure 1b). Two O atoms and one bridging F atom occupy the apical plane of the dimeric units, whereas the other F atoms are closely distributed along the equatorial planes of the octahedra.

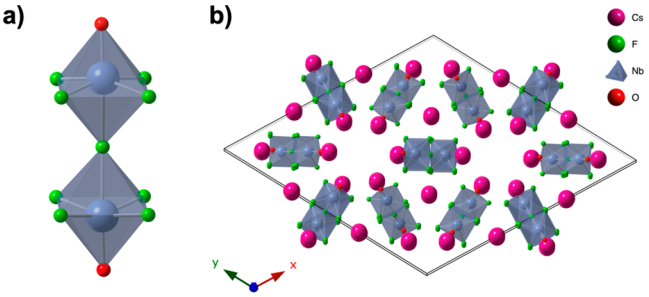

Figure 1. (a) View of a Nb dimer consisting of vertex-sharing $NbOF_5$ polyhedra. (b) View of a 3D framework structure containing isolated dinuclear anions and Cs ions that surround the channels.

$Cs_{10}(Nb_2O_2F_9)_3F$ and $Cs_{9.4}K_{0.6}(Nb_2O_2F_9)_3F$. The asymmetric unit in $P\bar{3}m1$ consists of 5 Cs atoms, 3 Nb atoms, 3 O atoms, and 10 unique F atoms. The $Nb_2O_2F_9$ dimers create infinite channels that are occupied by disordered species (Figures 2 and 3). These species are modeled as one F per channel-unit cell, which is in good agreement with the reported analogues.[36] The Cs3−Cs5 atoms surround a

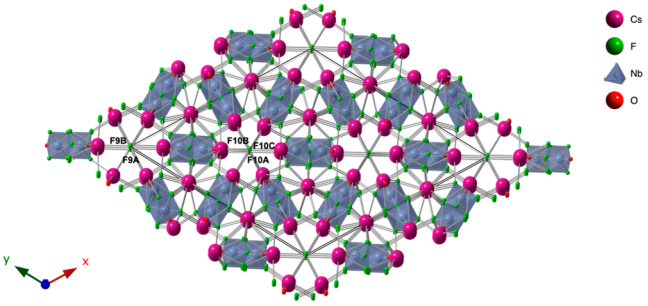

Figure 2. View of a 3D framework of $Cs_{10}(Nb_2O_2F_9)_3F$ that contains infinite channels that are occupied by disordered F^- ions. The black box outlines the unit cell.

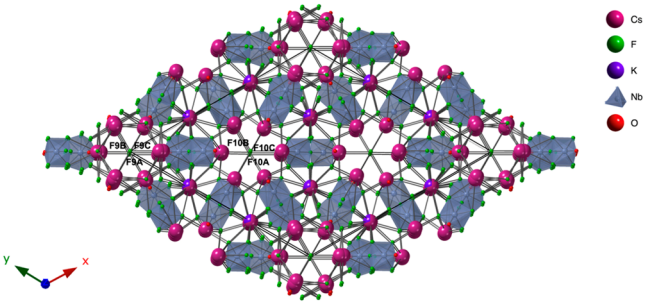

Figure 3. View of a 3D framework of $Cs_{9.4}K_{0.6}(Nb_2O_2F_9)_3F$ that contains infinite channels that are occupied by disordered F^- ions. The mixed-occupancy Cs/K site is shown as mixed pink/purple. The black box outlines the unit cell.

https://doi.org/10.1021/acs.inorgchem.1c03787
Inorg. Chem. 2022, 61, 3256−3262

hexagonal channel in the *ab* plane, but the Cs1 and Cs2 atoms connect the neighboring dimeric units to form a 3D framework structure. The F1−F8 atoms occupy the framework; however, the free fluoride ions, F9 and F10, are located in the hexagonal channels created by $[Nb_2O_2F_9]^{3-}$ dimeric units. The channel occupants in each case are highly disordered and were modeled as either two or three unique, partially occupied F sites. In agreement with previous reports of this structure type[36] and charge balance, the total occupancy of each channel was fixed to one F per channel. IR data (Figure S4) exhibited no evidence of O−H stretching, and the reactions were performed in a brand new PTFE liner, thus indicating that neither H_2O nor Cl^- is present in the channels of $Cs_{10}(Nb_2O_2F_9)_3F$ and $Cs_{9.4}K_{0.6}(Nb_2O_2F_9)_3F$. In the case of $Cs_{9.4}K_{0.6}(Nb_2O_2F_9)_3F$, the K atoms are substituted onto the Cs5 site and form a hexagonal tunnel in which the disordered fluoride ions F10 reside; however, the Cs3 and Cs4 sites are pure and surround the disordered fluoride ions F9 located in the other channels.

$Cs_{10}(Nb_2O_2F_9)_3Cl$. The asymmetric unit consists of five independent Cs atoms, three Nb atoms, eight F atoms, three O atoms, and five independent, but disordered and partially occupied, Cl atoms. This compound is isostructural with $Cs_{10}(Nb_2O_2F_9)_3F$ and $Cs_{9.4}K_{0.6}(Nb_2O_2F_9)_3F$; however, the $[Cs_{10}(Nb_2O_2F_9)_3]^+$ framework surrounds 1D channels parallel to [001] that are filled with disordered chloride ions (Figure 4). Cl1A is located at the origin (1a, −3m. site

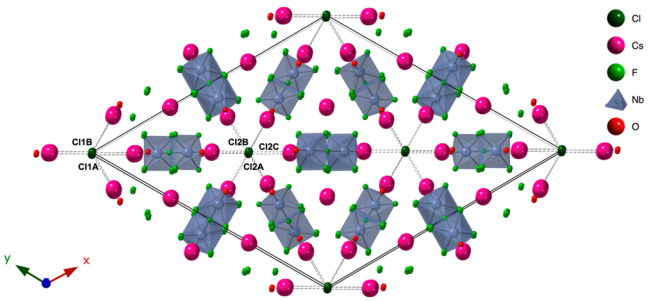

Figure 4. View of 3D framework of $Cs_{10}(Nb_2O_2F_9)_3Cl$ that contains 1D channels occupied by disordered chloride ions. The black box outlines the unit cell.

symmetry); a minor disorder component observed near Cl1A occupies site 2c (3m. symmetry, atom Cl1B). The Cl1 occupancies refined to Cl1A/Cl1B = 0.72(1)/0.14(1). Two Cl1B atoms are generated by symmetry per one Cl1A, for 1 total Cl per Cl1 disorder grouping. Disordered chloride ions Cl2A−C in the channels at ($^2/_3$, $^1/_3$, z) are on site 2d (3m. site symmetry). The Cl2 occupancies refined to Cl2A = 0.34(2), Cl2B = 0.38(2), and Cl2C = 0.28(2). Cl^- was not expected, but displacement parameters of the channel species, a Cs−Cl distance of 3.4 Å, and the achievement of a charge-balanced composition are consistent with Cl^-, and not F^- or $H_2O/OH^-/O^{2-}$ or a cation.

Luminescence Properties. The excitation and emission spectra of $Cs_{10}(Nb_2O_2F_9)_3F$ at room temperature are shown in Figure 5. When excited by UV light using an excitation wavelength of 248 nm, $Cs_{10}(Nb_2O_2F_9)_3F$ exhibits a broad emission spectrum with maxima at 440 nm. The emission spectrum of this material, containing Nb as an intrinsic luminescence center, is assumed to be mainly governed by the charge-transfer transition localized within the short Nb−O bonds of the $[Nb_2O_2F_9]^{3-}$ dimers.[21,22] This UV charge-transfer transition is believed to go from the anionic O 2p ligands to the cationic Nb 4d metal ion but not from the F 2p ligands because of the high electronegativity of F.

Reports in the literature indicate that the luminescence mechanisms of quaternary Cs_2NbOF_5 and $BaNbOF_5$ are attributed to the charge-transfer transitions of the Nb−O bonds in the $[NbOF_5]^{2-}$ units.[21,22] This has also been observed in other materials, such as $Cs_2WO_2F_4$ and $K_2NaTiOF_5$, consisting of $[WO_2F_4]^{2-}$ and $[TiOF_5]^{3-}$ building units, respectively.[37,38] Blasse et al. have reported

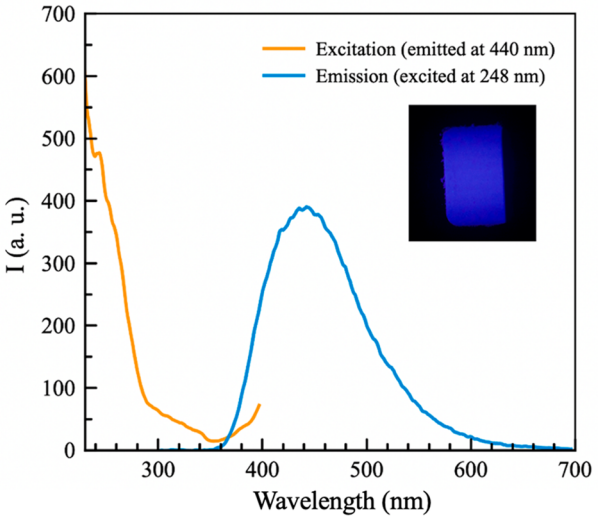

Figure 5. Excitation and emission spectra of $Cs_{10}(Nb_2O_2F_9)_3F$.

on ternary-layered niobate compounds, KNb_3O_8 and $K_4Nb_6O_{17}$, in which the emission arises from the short localized niobyl (Nb−O) bonds within the corner- and edge-sharing NbO_6 octahedral complexes.[39] There are related reports suggesting that the short Ti−O bonds within the isolated titanate octahedra similarly have a significant impact on the optical properties of titanates.[40] Moreover, the broad band emission in the niobium oxyphosphate $(NbO)_2P_4O_{13}$, encompassing the range of 350−600 nm, is attributed to the O 2p to Nb 4d charge-transfer transitions.[41] Therefore, one can presume that the emission in $Cs_{10}(Nb_2O_2F_9)_3F$, $Cs_{9.4}K_{0.6}(Nb_2O_2F_9)_3F$, and $Cs_{10}(Nb_2O_2F_9)_3Cl$ is also due to the charge-transfer transition of the Nb−O bonds within the $[Nb_2O_2F_9]^{3-}$ dimers, which causes the material to be luminescent.

As shown in Figure 6, $Cs_{10}(Nb_2O_2F_9)_3F$ visibly scintillates blue under Cu Kα X-ray irradiation within our Rigaku Ultima PXRD

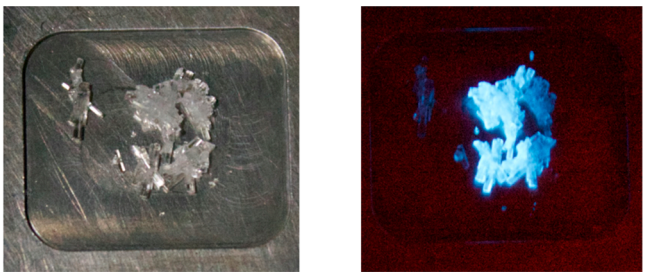

Figure 6. Optical images of (left) ground crystals of $Cs_{10}(Nb_2O_2F_9)_3F$ in the absence of X-rays and (right) scintillating ground crystals upon exposure to Cu Kα X-rays.

diffractometer. The scintillation responses of powdered $Cs_{10}(Nb_2O_2F_9)_3F$, $Cs_{9.4}K_{0.6}(Nb_2O_2F_9)_3F$, and $Cs_{10}(Nb_2O_2F_9)_3Cl$ were investigated under X-ray irradiation (RL measurements). These materials exhibit broad emission bands that peaked at ∼460 nm due to blue emission from the $[Nb_2O_2F_9]^{3-}$ dimers. Figure 7 shows the trend of the temperature dependence of the RL measurements of $Cs_{10}(Nb_2O_2F_9)_3F$, which exhibits a fast, continuous decrease in the intensity that reached about 50% of the original intensity already at around 70 °C and full thermal quenching at around 200 °C. This is more clearly seen in the peak intensity at 462 nm versus temperature plot (Figure 8). No shift of the peak position was observed as a function of the temperature. Integral RL emission at room temperature was about 4% of BGO powder. The RL spectra of $Cs_{9.4}K_{0.6}(Nb_2O_2F_9)_3F$ and $Cs_{10}(Nb_2O_2F_9)_3Cl$ are shown in Figure 9,

https://doi.org/10.1021/acs.inorgchem.1c03787
Inorg. Chem. 2022, 61, 3256−3262

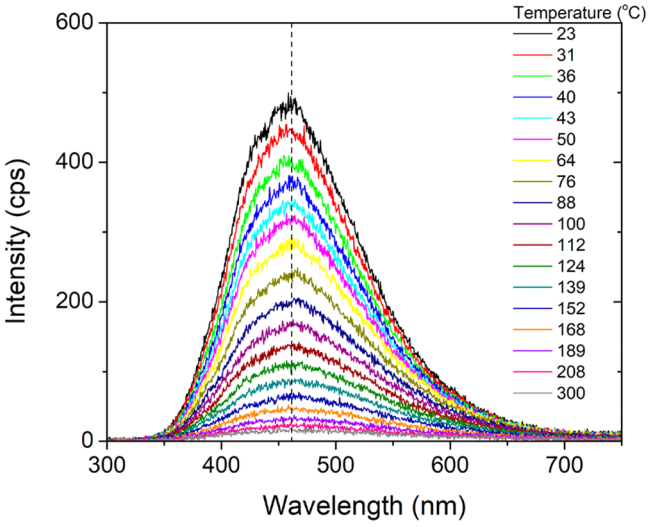

Figure 7. RL emission intensity as a function of the temperature for $Cs_{10}(Nb_2O_2F_9)_3F$ under broad-range W X-ray emission.

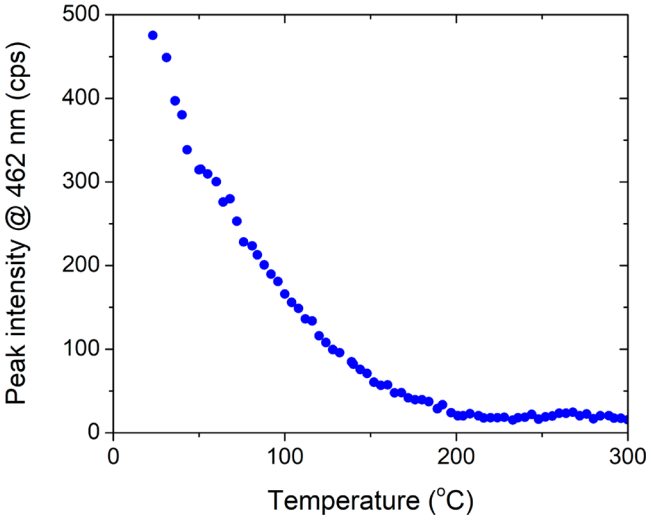

Figure 8. Peak intensity of the main line at 462 nm as a function of the temperature for $Cs_{10}(Nb_2O_2F_9)_3F$.

with both exhibiting lower intensity scintillation than $Cs_{10}(Nb_2O_2F_9)_3F$.

Thermogravimetric Analysis (TGA). The thermal stability of $Cs_{10}(Nb_2O_2F_9)_3F$ was evaluated using TGA up to 1000 °C under a N_2 gas flow (Figure 10). The TGA data show that the compound does not undergo decomposition until approximately 600 °C, which illustrates the high thermal stability of $Cs_{10}(Nb_2O_2F_9)_3F$. Between 600 and 1000 °C, the compound loses ~50% mass, which results in the formation of $Cs_2Nb_4O_{11}$ based on PXRD analysis (Figure S5). We conclude that $Cs_{10}(Nb_2O_2F_9)_3F$ degrades by liberating F upon heating above 600 °C.

CONCLUSION

In summary, we have successfully prepared three new disordered Nb-based mixed-anion oxide−fluorides, $Cs_{10}(Nb_2O_2F_9)_3F$, $Cs_{9.4}K_{0.6}(Nb_2O_2F_9)_3F$, and $Cs_{10}(Nb_2O_2F_9)_3Cl$, by employing a mild hydrothermal route. The crystal structures of all three compounds contain $[Nb_2O_2F_9]^{3-}$ dimers, formed by two corner-sharing $[NbOF_5]^{2-}$ octahedra that are linked together by Cs ions to form a 3D framework structure. These compounds luminesce

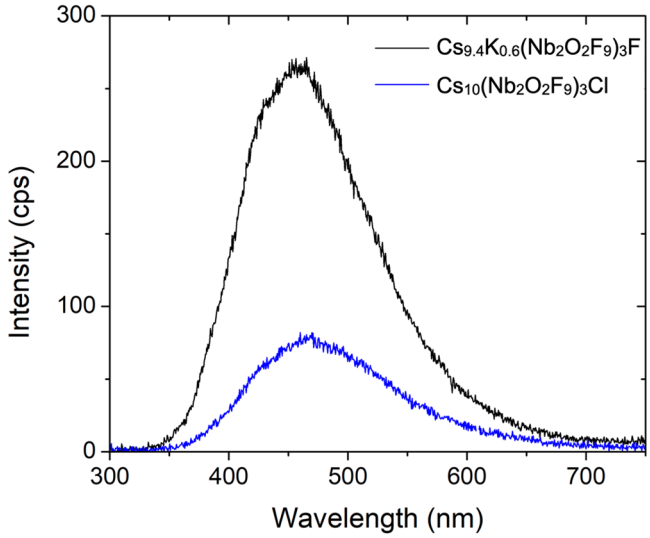

Figure 9. RL emission spectra of $Cs_{10}(Nb_2O_2F_9)_3Cl$ and $Cs_{9.4}K_{0.6}(Nb_2O_2F_9)_3F$ under broad-range W X-ray emission.

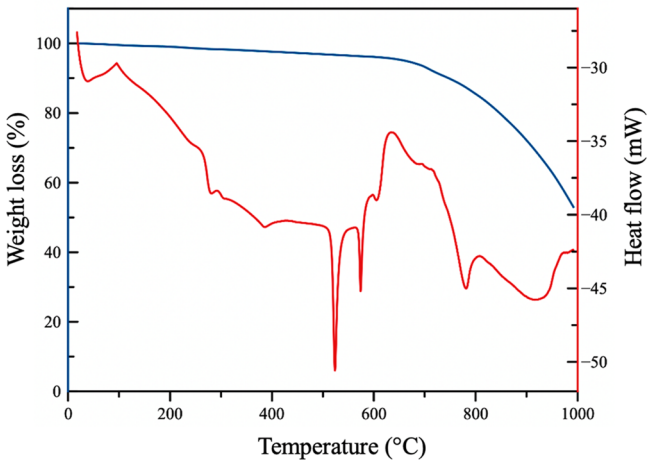

Figure 10. TGA diagram for $Cs_{10}(Nb_2O_2F_9)_3F$.

blue under UV excitation at room temperature and exhibit broad band emissions. Single crystals of $Cs_{10}(Nb_2O_2F_9)_3F$ emit an intense blue color upon irradiation with laboratory X-rays and the integral RL emission was about 4% of BGO powder. The RL emission intensity of the $Cs_{10}(Nb_2O_2F_9)_3F$ compound was thermally quenched at about 200 °C. On the other hand, the $Cs_{10}(Nb_2O_2F_9)_3F$ compound exhibited excellent thermal stability up to 600 °C. Our investigation demonstrates the ability to synthesize new mixed-anion niobium oxide−fluorides that are thermally stable and exhibit significant X-ray scintillation.

ASSOCIATED CONTENT

Supporting Information

The Supporting Information is available free of charge at https://pubs.acs.org/doi/10.1021/acs.inorgchem.1c03787.

PXRD patterns and FTIR data (PDF)

Accession Codes

CCDC 2123001−2123003 contain the supplementary crystallographic data for this paper. These data can be obtained free of charge via www.ccdc.cam.ac.uk/data_request/cif, or by

https://doi.org/10.1021/acs.inorgchem.1c03787
Inorg. Chem. 2022, 61, 3256−3262

emailing data_request@ccdc.cam.ac.uk, or by contacting The Cambridge Crystallographic Data Centre, 12 Union Road, Cambridge CB2 1EZ, UK; fax: +44 1223 336033.

AUTHOR INFORMATION

Corresponding Author

Hans-Conrad zur Loye − *Department of Chemistry and Biochemistry, University of South Carolina, Columbia, South Carolina 29208, United States;* orcid.org/0000-0001-7351-9098; Email: zurloye@mailbox.sc.edu

Authors

Gyanendra B. Ayer − *Department of Chemistry and Biochemistry, University of South Carolina, Columbia, South Carolina 29208, United States*

Gregory Morrison − *Department of Chemistry and Biochemistry, University of South Carolina, Columbia, South Carolina 29208, United States;* orcid.org/0000-0001-9674-9224

Mark D. Smith − *Department of Chemistry and Biochemistry, University of South Carolina, Columbia, South Carolina 29208, United States*

Luiz G. Jacobsohn − *Department of Materials Science and Engineering, Clemson University, Clemson, South Carolina 29634, United States*

Complete contact information is available at: https://pubs.acs.org/10.1021/acs.inorgchem.1c03787

Notes

The authors declare no competing financial interest.

ACKNOWLEDGMENTS

Financial support for this work provided by the National Science Foundation under Grants DMR-1806279 and DMR-1653016 is gratefully acknowledged. Syntheses, structure determination, PL, and TGA were performed at University of South Carolina. RL measurements were performed at Clemson University.

REFERENCES

(1) Chen, Q.; Wu, J.; Ou, X.; Huang, B.; Almutlaq, J.; Zhumekenov, A. A.; Guan, X.; Han, S.; Liang, L.; Yi, Z.; Li, J.; Xie, X.; Wang, Y.; Li, Y.; Fan, D.; Teh, D. B. L.; All, A. H.; Mohammed, O. F.; Bakr, O. M.; Wu, T.; Bettinelli, M.; Yang, H.; Huang, W.; Liu, X. All-inorganic perovskite nanocrystal scintillators. *Nature* **2018**, *561*, 88−93.

(2) van Eijk, C. W. E. Inorganic Scintillators in Medical Imaging. *Phys. Med. Biol.* **2002**, *47*, R85−R106.

(3) Eriksson, L.; Melcher, C. L.; Eriksson, M.; Rothfuss, H.; Grazioso, R.; Aykac, M. Design Considerations of Phoswich Detectors for High Resolution Positron Emission Tomography. *IEEE Trans. Nucl. Sci.* **2009**, *56*, 182−188.

(4) Duclos, S. J.; Greskovich, C. D.; Lyons, R. J.; Vartuli, J. S.; Hoffman, D. M.; Riedner, R. J.; Lynch, M. J. Development of the HiLight scintillator for computed tomography medical imaging. *Nucl. Instrum. Methods Phys. Res., Sect. A* **2003**, *505*, 68−71.

(5) Melcher, C. L.; Schweitzer, J. S. A promising new scintillator: cerium-doped lutetium oxyorthosilicate. *Nucl. Instrum. Methods Phys. Res., Sect. A* **1992**, *314*, 212−214.

(6) West, H. I.; Meyerhof, W. E.; Hofstadter, R. Detection of X-rays by means of NaI(Tl) scintillation counters. *Phys. Rev.* **1951**, *81*, 141−142.

(7) Cha, B. K.; Shin, J.-H.; Bae, J. H.; Lee, C.-h.; Chang, S.; Kim, H. K.; Kim, C. K.; Cho, G. Scintillation characteristics and imaging performance of CsI:Tl thin films for X-ray imaging applications. *Nucl. Instrum. Methods Phys. Res., Sect. A* **2009**, *604*, 224−228.

(8) Liu, B.; Shi, C.; Yin, M.; Fu, Y.; Zhang, G.; Ren, G. Luminescence and energy transfer processes in $Lu_2SiO_5:Ce^{3+}$ scintillator. *J. Lumin.* **2006**, *117*, 129−134.

(9) Stand, L.; Zhuravleva, M.; Chakoumakos, B.; Johnson, J.; Loyd, M.; Wu, Y.; Koschan, M.; Melcher, C. L. Crystal Growth and Scintillation Properties of Eu^{2+} doped Cs_4CaI_6 and Cs_4SrI_6. *J. Cryst. Growth.* **2018**, *486*, 162−168.

(10) Laguta, V. V.; Nikl, M.; Rosa, J.; Grinyov, B. V.; Nagornaya, L. L.; Tupitsina, I. A. Electron spin resonance study of self-trapped holes in $CdWO_4$ scintillator crystals. *J. Appl. Phys.* **2008**, *104*, 103525.

(11) Takagi, K.; Oi, T.; Fukazawa, T.; Ishii, M.; Akiyama, S. Improvement in the scintillation conversion efficiency of $Bi_4Ge_3O_{12}$ single crystals. *J. Cryst. Growth* **1981**, *52*, 584−587.

(12) Morrison, G.; Latshaw, A. M.; Spagnuolo, N. R.; zur Loye, H.-C. Observation of Intense X-ray Scintillation in a Family of Mixed Anion Silicates, $Cs_3RESi_4O_{10}F$ (RE = Y, Eu−Lu), Obtained via an Enhanced Flux Crystal Growth Technique. *J. Am. Chem. Soc.* **2017**, *139*, 14743−14748.

(13) Eagleman, Y. D.; Bourret-Courchesne, E.; Derenzo, S. E. Room-temperature scintillation properties of cerium-doped REOX (RE = Y, La, Gd, and Lu; X = F, Cl, Br, and I). *J. Lumin.* **2011**, *131*, 669−675.

(14) Passuello, T.; Piccinelli, F.; Trevisani, M.; Giarola, M.; Mariotto, G.; Marciniak, L.; Hreniak, D.; Guzik, M.; Fasoli, M.; Vedda, A.; Jary, V.; Nikl, M.; Causin, V.; Bettinelli, M.; Speghini, A. Structural and optical properties of Vernier phase lutetium oxyfluorides doped with lanthanide ions: interesting candidates as scintillators and X-ray phosphors. *J. Mater. Chem.* **2012**, *22*, 10639−10649.

(15) Ayer, G. B.; Klepov, V. V.; Smith, M. D.; Hu, M.; Yang, Z.; Martin, C. R.; Morrison, G.; zur Loye, H.-C. $BaWO_2F_4$: a mixed anion X-ray scintillator with excellent photoluminescence quantum efficiency. *Dalton Trans.* **2020**, *49*, 10734−10739.

(16) Karsu, E. C.; Popovici, E. J.; Ege, A.; Morar, M.; Indrea, E.; Karali, T.; Can, N. Luminescence study of some yttrium tantalate-based phosphors. *J. Lumin.* **2011**, *131*, 1052−1057.

(17) Voloshyna, O. V.; Boiaryntseva, I. A.; Baumer, V. N.; Ivanov, A. I.; Korjik, M. V.; Sidletskiy, O. T. New, dense, and fast scintillators based on rare-earth tantalo-niobates. *Nucl. Instrum. Methods Phys. Res., Sect. A* **2014**, *764*, 227−231.

(18) Yu, R.; Fan, A.; Yuan, M.; Li, T.; Wang, J. Observation of intrinsic emission in β-$BiNbO_4$ available for excitation of both UV light and high energy irradiation. *Phys. Chem. Chem. Phys.* **2016**, *18*, 23702−23708.

(19) Bharathy, M.; Rassolov, V. A.; zur Loye, H.-C. Crystal Growth of $Sr_3NaNbO_6$and Sr_3NaTaO_6: New Photoluminescent Oxides. *Chem. Mater.* **2008**, *20*, 2268−2273.

(20) Roof, I. P.; Jagau, T.-C.; Zeier, W. G.; Smith, M. D.; zur Loye, H.-C. Crystal Growth of a New Series of Complex Niobates, $LnKNaNbO_5$ (Ln = La, Pr, Nd, Sm, Eu, Gd, and Tb): Structural Properties and Photoluminescence. *Chem. Mater.* **2009**, *21*, 1955−1961.

(21) Srivastava, A. M.; Ackerman, J. F. Synthesis and Luminescence properties of $BaNbOF_5$ with isolated $[NbOF_5]^{2-}$ Octahedra. *Chem. Mater.* **1992**, *4*, 1011−1013.

(22) Srivastava, A. M.; Ackerman, J. F. Synthesis and luminescence properties of Cs_2NbOF_5 and Cs_2NbOCl_5 with isolated $[NbOX_5]^{-2}$ (X = F^-, Cl^-) octahedra. *Mater. Res. Bull.* **1991**, *26*, 443−448.

(23) *APEX3*, version 2019.1-0, and *SAINT+*, version 8.40A; Bruker Nano, Inc.: Madison, WI, 2019.

(24) Krause, L.; Herbst-Irmer, R.; Sheldrick, G. M.; Stalke, D. Comparison of Silver and Molybdenum Microfocus X-Ray Sources for Single-Crystal Structure Determination. *J. Appl. Crystallogr.* **2015**, *48* (1), 3−10.

(25) Sheldrick, G. M. Crystal Structure Refinement with *SHELXT*. *Acta Crystallogr., Sect. A: Struct. Chem.* **2015**, *71* (1), 3−8.

(26) Sheldrick, G. M. Crystal Structure Refinement with *SHELXL*. *Acta Crystallogr., Sect. C: Struct. Chem.* **2015**, *71* (1), 3−8.

(27) *OLEX2*: a complete structure solution, refinement and analysis program: Dolomanov, O. V.; Bourhis, L. J.; Gildea, R. J.; Howard, J. A. K.; Puschmann, H. *J. Appl. Crystallogr.* **2009**, *42*, 339−341.
(28) Ayer, G. B.; Klepov, V. V.; Pace, K. A.; zur Loye, H.-C. Quaternary Cerium(IV) Containing Fluorides Exhibiting Ce_3F_{16} Sheets and Ce_6F_{30} Frameworks. *Dalton Trans.* **2020**, *49*, 5898−5905.
(29) Hancock, J. C.; Nisbet, M. L.; Zhang, W.; Halasyamani, P. S.; Poeppelmeier, K. R. Periodic Tendril Perversion and Helices in the $AMoO_2F_3$ (A = K, Rb, NH_4, Tl) Family. *J. Am. Chem. Soc.* **2020**, *142*, 6375−6380.
(30) Klepov, V. V.; Pace, K. A.; Calder, S.; Felder, J. B.; zur Loye, H.-C. 3d-Metal Induced Magnetic Ordering on U(IV) Atoms as a Route toward U(IV) Magnetic Materials. *J. Am. Chem. Soc.* **2019**, *141*, 3838−3842.
(31) Pace, K. A.; Klepov, V. V.; Deason, T. K.; Smith, M. D.; Ayer, G. B.; Diprete, D. P.; Amoroso, J. W.; zur Loye, H.-C. *Chem. Eur. J.* **2020**, *26*, 12941−12944.
(32) Aldous, D. W.; Goff, R. J.; Attfield, J. P.; Lightfoot, P. Novel vanadium(IV) oxyfluorides with 'spin-ladder'-like structures, and their relationship to $(VO)_2P_2O_7$. *Inorg. Chem.* **2007**, *46*, 1277−1282.
(33) Ayer, G. B.; Klepov, V. V.; Smith, M. D.; zur Loye, H.-C. Mild Hydrothermal Synthesis of the Complex Hafnium-Containing Fluorides $Cs_2[M(H_2O)_6][Hf_2F_{12}]$ (M = Ni, Co, Zn), $CuHfF_6(H_2O)_4$, and $Cs_2Hf_3Mn_3F_{20}$ Based on HfF_7 and HfF_6 Coordination Polyhedra. *Inorg. Chem.* **2019**, *58*, 13049−13057.
(34) Agulyansky, A. *The Chemistry of Tantalum and Niobium Fluoride Compounds*, 1st ed.; Elsevier: New York, 2005; p 407.
(35) Savchenko, G. S.; Tananaev, I. V. Research in the field of complex fluoride salts of tantalum and niobium. *Zh. Prikl. Him.* **1947**, *20* (5), 385−390.
(36) Udovenko, A. A.; Laptash, N. M. Dinuclear oxofluorometallates as a new structural type of d(0) transition metal oxofluoride compound. *Acta Crystallogr. Sect. B: Struct. Sci., Cryst. Eng. Mater.* **2012**, *68*, 602−609.
(37) Srivastava, A. M.; Ackerman, J. F. Structure and luminescence of $Cs_2WO_2F_4$: Efficient luminescence of isolated $[WO_2F_4]^{-2}$ octahedra. *J. Solid State Chem.* **1992**, *98*, 144−150.
(38) Blasse, G.; Dirksen, G. J.; Pausewang, G. J.; Schmidt, R. Vibrational structure in the luminescence of the $[TiOF_5]^{3-}$ octahedron. *J. Solid State Chem.* **1990**, *88*, 586−589.
(39) Kudo, A.; Sakata, T. Effect of Ion Exchange on Photoluminescence of Layered Niobates $K_4Nb_6O17$and KNb_3O_8. *J. Phys. Chem.* **1996**, *100*, 17323−17326.
(40) Bouma, B.; Blasse, G. Dependence of luminescence of titanates on their crystal structure. *J. Phys. Chem. Solids* **1995**, *56*, 261−265.
(41) Schildhammer, D.; Fuhrmann, G.; Petschnig, L. L.; Wurst, K.; Vitzthum, D.; Seibald, M.; Schottenberger, H.; Huppertz, H. Structural Redetermination and Photoluminescence Properties of the Niobium Oxyphosphate $(NbO)_2P_4O_{13}$. *Inorg. Chem.* **2017**, *56*, 2736−2741.

https://doi.org/10.1021/acs.inorgchem.1c03787
Inorg. Chem. 2022, 61, 3256−3262